Biophysical Journal
Article

Biophysical Society

The Role of Cholesterol in Driving IAPP-Membrane Interactions

Michele F. M. Sciacca,[1] Fabio Lolicato,[2,3] Giacomo Di Mauro,[2] Danilo Milardi,[1] Luisa D'Urso,[2] Cristina Satriano,[2] Ayyalusamy Ramamoorthy,[4,5,6,*] and Carmelo La Rosa[2,*]

[1]Istituto di Biostrutture e Bioimmagini, Consiglio Nazionale delle Ricerche, Catania, Italy; [2]Dipartimento di Scienze Chimiche, Università degli Studi di Catania, Catania, Italy; [3]Department of Physics, Tampere University of Technology, Tampere, Finland; [4]Biophysics and [5]Department of Chemistry, University of Michigan, Ann Arbor, Michigan; and [6]Institute for Advanced Study, Technische Universität München, Lichtenbergstrasse, Garching, Germany

ABSTRACT Our knowledge of the molecular events underlying type 2 diabetes mellitus—a protein conformational disease characterized by the aggregation of islet amyloid polypeptide (IAPP) in pancreatic β cells—is limited. However, amyloid-mediated membrane damage is known to play a key role in IAPP cytotoxicity, and therefore the effects of lipid composition on modulating IAPP-membrane interactions have been the focus of intense research. In particular, membrane cholesterol content varies with aging and consequently with adverse environmental factors such as diet and lifestyle, but its role in the development of the disease is controversial. In this study, we employ a combination of experimental techniques and in silico molecular simulations to shed light on the role of cholesterol in IAPP aggregation and the related membrane disruption. We show that if anionic POPC/POPS vesicles are used as model membranes, cholesterol has a negligible effect on the kinetics of IAPP fibril growth on the surface of the bilayer. In addition, cholesterol inhibits membrane damage by amyloid-induced poration on membranes, but enhances leakage through fiber growth on the membrane surface. Conversely, if 1:2 DOPC/DPPC raft-like model membranes are used, cholesterol accelerates fiber growth. Next, it enhances pore formation and suppresses fiber growth on the membrane surface, leading to leakage. Our results highlight a twofold effect of cholesterol on the amyloidogenicity of IAPP and help explain its debated role in type 2 diabetes mellitus.

INTRODUCTION

Type 2 diabetes mellitus (T2DM) is an increasingly alarming global health threat. To date, several reports have shown a clear link between dietary type and the risk of T2DM (1). Hyperlipidemia is one of the many nutritional factors that contribute to the etiopathogenesis of T2DM (2). Actually, the relationship between T2DM and obesity and high plasma levels of free fatty acids (FFAs) suggests that abnormal lipid metabolism may induce hyperglycemia and β-cell failure (3). In addition to FFAs, plasma cholesterol is often elevated in obese patients (4), and foods rich in cholesterol are normally considered to play a causative role in T2DM (5,6).

Cholesterol is a major component (30–50 mol %) of mammalian plasma and internal cell membranes (7,8). It is known to regulate glucose metabolism in adipocytes (9) by altering the properties of membrane microdomains (rafts) and by activating several transcription factors (10), but the molecular events that link cholesterol and T2DM remain to be elucidated. Cholesterol significantly affects membrane properties, participates in lipid bilayer packing, and contributes to the formation of lipid rafts, which float in the more-fluid lipid domains that are enriched in unsaturated hydrocarbon chains (11). Lipid rafts are also involved in the regulation of many cell signaling pathways by increasing the local concentration of specific proteins at selected membrane sites (11).

Islet amyloid polypeptide (IAPP) is a 37-residue peptide that is secreted by β-cells of the pancreatic islets of Langerhans (12). IAPP has a remarkable propensity to aggregate into insoluble amyloid fibrils, which are found in the islets of 90% of patients with T2DM (13). IAPP has a predominantly random coil structure in water (14). However, several studies have confirmed that IAPP forms an α-helical conformation in the N-terminal domain, with a rigid disulfide linkage bridging Cys2 and Cys7 (15–19). Other studies support the hypothesis that IAPP amyloid aggregation initiates with an α-helix to β-sheet conversion, and that this conversion may be accelerated by anionic lipid membranes (15,16,20,21).

Islet amyloid deposits are clearly linked to T2DM pathogenesis (22–25) but are also present in some nondiabetic individuals (17,26). Although some early studies showed that

Submitted January 21, 2016, and accepted for publication May 26, 2016.

*Correspondence: ramamoor@umich.edu or clarosa@unict.it

Editor: Francesca Marassi.

http://dx.doi.org/10.1016/j.bpj.2016.05.050

IAPP amyloid fibrils are toxic to β-cells (27), clinical evidence and subsequent reports have suggested that mature IAPP fibrils are inert and that the oligomeric intermediates are the most cytotoxic species (28). The oligomeric amyloid intermediates have been suggested to insert into and then disrupt the cell membrane by forming ion-channel structures (29–35), and cell membrane poration has been proposed to be a universal mechanism for amyloid toxicity (12,36). However, pore formation is not the only possible mechanism by which IAPP may permeabilize the cell membrane. A large number of experiments have provided evidence for nonspecific binding of amyloid oligomers to the lipid bilayer surface (37,38), and detergent-like membrane disruption by the growing amyloid fibrils on the lipid bilayer surface (39). More recently, it was proposed that these two mechanisms are not necessarily mutually exclusive and may be involved simultaneously in IAPP-mediated membrane damage (35,40). Other recent studies have reported on the pivotal role played by cholesterol in modulating the interaction of IAPP and lipidic membranes (41–43). It was observed that cholesterol catalyzes IAPP amyloid aggregation on the plasma membranes of PC12 cells (44). Furthermore, transgenic mice lacking Abca1 (ATP-binding cassette transporter 1, which removes excess cholesterol from cell membranes) exhibit an abnormal glucose tolerance (45,46). These findings point unequivocally to a key role played by membrane cholesterol in damaging pancreatic β-cells and, even more importantly, identify cholesterol as a potential pathogenic link between T2DM and atherosclerosis, the most common cause of death in people with diabetes. The presence of lipid rafts in pancreatic β-cells (47) and in human extracellular amyloid fibrils (48) further confirms the role of cholesterol in the pathogenesis of T2DM. Nevertheless, the effect of cholesterol on IAPP-mediated membrane-damage mechanisms is not well understood.

To address this issue, we employed a combination of molecular dynamics (MD) and experimental techniques to investigate the effect of cholesterol on IAPP-evoked membrane disruption using raft-like 1,2-dioleoyl-*sn*-glycero-3-phosphocholine/1,2-dipalmitoyl-*sn*-glycero-3-phosphocholine (DOPC/DPPC) and 1-palmitoyl-2-oleoyl-*sn*-glycero-3-phosphocholine/1-palmitoyl-2-oleoyl-*sn*-glycero-3-phospho-L-serine sodium salt (POPC/POPS) large unilamellar vesicles (LUVs). Our data demonstrate that the presence of cholesterol strongly modulates the mechanism of membrane disruption induced by IAPP. In particular, we observed an enhancement of pore formation in raft-like DOPC/DPPC membranes and an increase in a detergent-like mechanism in POPC/POPS LUVs.

MATERIALS AND METHODS

Materials

Human IAPP (IAPP) was purchased from Bachem (Bubendorf, Switzerland) with a purity of >99%. POPC, POPS, DPPC, and DOPC were purchased from Avanti Polar Lipids (Alabaster, AL). Cholesterol, 6-carboxyfluorescein, thioflavin T (ThT), and 1,1,1,3,3,3-hexa-fluoro-2-propanol (HFIP) were purchased from Sigma-Aldrich (St. Louis, MO) with a purity of 99%.

MD simulations

All-atom MD simulations were performed for four different membrane systems. Each system had the same 1:2 molar ratio for DOPC/DPPC but different cholesterol concentrations (0, 20, 30, and 40 mol %). POPC/POPS (7:3) was also simulated. The initial structure of the lipid bilayer was obtained by using the CHARMM-Gui (49–51) website. All simulated bilayers were symmetric with regard to lipid composition and were adequately hydrated with 32 water molecules per lipid in the presence of 0.1 M NaCl. The overall charge neutrality was preserved by adding Cl^- counterions to the lipid bilayer. The atomistic simulations were carried out using GROMACs 5.0.4. The CHARMM36 force field (52,53) was used. Water molecules were described using the TIP3P model (54). The temperature was maintained at 298 K for all simulations to mimic the experimental setup, using a Nosé-Hoover thermostat (55,56) with a coupling constant of 1 ps. The temperatures of the solute and solvent were controlled independently. Periodic boundary conditions were used in all three directions. The pressure was kept constant with a semi-isotropic scheme, meaning that the pressure in the x and y directions was coupled separately from the pressure in the z direction. A Parrinello-Rahman barostat (57,58) was used to keep the pressure at 1 atm, with a pressure coupling constant of 5 ps and a compressibility of 4.5×10^{-5} bar^{-1}. Long-range electrostatic interactions beyond the nonbonded interaction cutoff of 1.2 nm were treated by using the particle mesh Ewald scheme and the Verlet cutoff scheme as recommended elsewhere (59). The LINCS algorithm (60) was used to constrain hydrogen bonds, allowing a time step of 2 fs. The systems were first energy minimized using a steepest-descent algorithm, followed by an equilibration simulation in the isothermal isobaric (NpT) ensemble until a stable average area per molecule was obtained. MD simulations of all of the lipid bilayer systems were carried out for 300 ns. The first 150 ns were considered a sufficient equilibration time and only the last 150 ns of each trajectory were included in the analyses. For analysis and visualization, the VMD package (61) and GROMACS (62) analysis tools were used. The bilayer thickness was calculated using Memb plugin 1.1 (63), a VMD plugin.

Preparation of model membranes

In this study, we used LUVs composed of POPC/POPS (7:3 molar ratio) or DOPC/DPPC (1:2 molar ratio). For each set of LUVs, we prepared samples containing increasing amounts of cholesterol (0, 20, 30, and 40 mol %). Model membranes were prepared as described elsewhere (64). Briefly, aliquots of lipid stock solutions in chloroform were dried by using a stream of dry nitrogen gas and evaporated under high vacuum to dryness in a round-bottomed flask. To obtain multilamellar vesicles (MLVs), the resulting lipid film was hydrated with an appropriate amount of phosphate buffer (10 mM buffer, 100 mM NaCl, pH 7.4) and dispersed by vigorous stirring in a water bath. LUVs were obtained by extruding the MLVs through polycarbonate filters (pore size = 100 nm; Nuclepore, Pleasanton, CA) mounted in a mini-extruder (Avestin, Ottawa, Canada) fitted with two 0.5 mL Hamilton gas-tight syringes (Hamilton, Reno, NV). The samples were typically subjected to 23 passes through two filters in tandem, as recommended elsewhere (65). An odd number of passages were performed to avoid contamination of the sample by vesicles that might not have passed through the filter.

IAPP preparation

To prevent the presence of any preformed aggregates, IAPP was initially dissolved in HFIP at a concentration of 1 mg/mL and then lyophilized

overnight. For dye leakage and ThT experiments, the lyophilized powder was dissolved in dimethyl sulfoxide to obtain a stock solution with a final concentration of 250 μM. Each stock solution of IAPP was used immediately after preparation. For circular dichroism (CD) and atomic force microscopy (AFM) experiments, the lyophilized powder was dissolved in 100 microL 0.1 M HCl at 4°C to a final concentration of 100 microM (stock solution). Aliquots of stock solution were then added to the buffer (pH 7.4) to a final IAPP concentration of 10 microM.

ThT measurements

The kinetics of amyloid formation was measured via the well-known ThT assay. Samples were prepared by adding 1 μL of the 250 μM dimethyl sulfoxide peptide stock solution to 100 μL of 10 mM phosphate buffer solution (pH 7.4, 100 mM NaCl, containing 10 μM ThT). Experiments were carried out in Corning 96-well nonbinding surface plates. Time traces were recorded using a Varioskan plate reader (ThermoFisher, Waltham, MA) with $\lambda_{ecc} = 440$ nm and $\lambda_{em} = 485$ nm at 25°C, and the samples were shaken for 10 s before each reading.

Membrane leakage experiments

Membrane leakage experiments were performed by measuring the leakage of 6-carboxyfluorescein dye from LUVs. Dye-filled LUVs were prepared by hydrating the dry lipid film with the solution containing 6-carboxyfluorescein (70 mM 6-carboxyfluorescein, pH 7.4) according to the procedure described above. To remove nonencapsulated 6-carboxyfluorescein, we placed the solution containing LUVs on a Sephadex G50 column (Sigma-Aldrich) and eluted it using the phosphate buffer solution to ensure that the osmotic pressure would not destabilize the LUVs over time. We checked the final concentration of lipids by using the Stewart assay (66). Membrane damage was quantified by the increase in fluorescence emission intensity of 6-carboxyfluorescein due to its dilution (dequenching) in buffer as a consequence of membrane leakage, as described elsewhere (67).

CD experiments

We evaluated the binding of IAPP with lipid vesicles by titrating a fresh solution of 10 μM IAPP with LUVs of varying membrane composition. A conformational transition from random coil to α-helix occurs when IAPP binds a membrane. Thus, a decrease in the ellipticity at 222 nm can be used to evaluate the affinity of IAPP for binding with a membrane (67). We carried out measurements by recording the ellipticity at 222 nm for 30 s for each lipid/protein ratio, and then plotted the average data as a function of lipid concentration. All measurements were carried out in 10 mM phosphate buffer solution (100 mM NaF, pH 7.4) at $T = 25$°C.

AFM measurements

Liquid imaging in the AC mode was performed with a Cypher atomic force microscope (Asylum Research/Oxford Instruments, Goleta, CA). We used BioLever Mini BL-AC40TS (Olympus, Tokyo, Japan) AFM probes with 30 kHz resonance frequency in liquid and 0.1 N m^{-1} spring constant (free oscillation amplitude of 20 nm; set point at ~70% of the free oscillation amplitude; scan rate 2.44 Hz). For supported lipid bilayer (SLB) deposition, freshly cleaved mica dishes were immersed in the lipid vesicle solutions, sonicated for 30 min, and then copiously rinsed with 10 mM phosphate-buffered saline. For imaging of lipid bilayer-fibril interactions, a total of 2 μL of IAPP solution was spotted on the SLB on mica samples covered by 100 μL of phosphate-buffered saline to obtain a final IAPP concentration of 10 μM.

RESULTS

Cholesterol enhances the kinetics of IAPP fiber formation in raft-containing 1:2 DOPC/DPPC lipid bilayers

We initially examined the kinetics of IAPP fiber formation in the presence of 250 μM (1:2 mol ratio) DOPC/DPPC membranes by varying the amount of cholesterol from 0 to 40 mol %. These lipid membranes are characterized by the presence of cholesterol-rich microdomains that resemble raft-like structures with higher thickness and decreased fluidity (68). The presence of cholesterol in DOPC/DPPC membranes significantly affected the amyloid fiber-formation kinetics, as shown by ThT curves (Fig. 1 *A*). In particular, the lag time was significantly reduced as the cholesterol concentration was increased, and the presence of cholesterol also reduced the fiber elongation rate (i.e., the slope of the ThT fluorescence curve). Moreover, the increasing cholesterol content reduced the

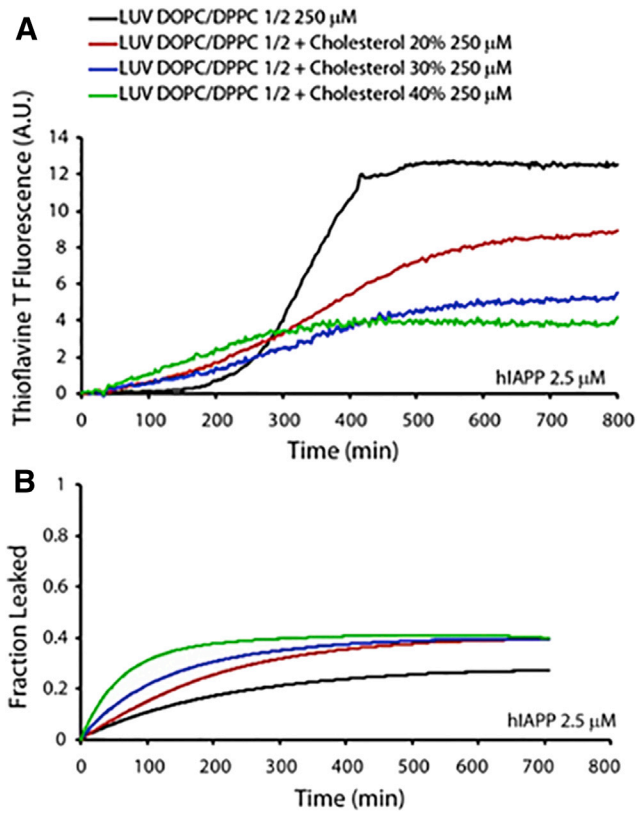

FIGURE 1 IAPP fiber-formation kinetics and disruption of DOPC/DPPC LUVs. (*A*) Fiber formation measured in the presence of 250 μM of 1:2 DOPC/DPPC LUVs containing 0% (*black*), 20% (*red*), 30% (*blue*), and 40% (*green*) cholesterol. IAPP concentration was 2.5 μM for all samples. (*B*) IAPP induced release of 6-carboxyfluorescein from LUVs composed of 250 μM (1:2 molar ratio) DOPC/DPPC containing 0% (*black*), 20% (*red*), 30% (*blue*), and 40% (*green*) cholesterol. Experiments were performed at 25°C in 10 mM phosphate buffer, 100 mM NaCl, pH 7.4. All results are the average of three experiments. To see this figure in color, go online.

total amount of fibers. This behavior could be explained by the increased negative curvature, which is associated with raft domains and is known to promote peptide binding and fiber formation (67).

Cholesterol enhances pore formation in raft-containing LUVs

Previous studies have shown that IAPP induces lipid membrane disruption through a two-step mechanism (67,69). The first step is correlated with pore formation, and the second step is a detergent-like mechanism of membrane disruption due to the growth of amyloid fibers on the surface of the lipid bilayer (69). To gain more insights into IAPP-induced membrane disruption, we performed dye-leakage experiments on raft-containing DOPC/DPPC LUVs prepared with various amounts of cholesterol (Fig. 1 *B*). We observed dye release immediately after the addition of IAPP, well before fiber formation occurred. Of note, according to our MD simulations (vide infra) and previous reports, the accumulation of cholesterol in raft domains results in differences in the thickness of the lipid-ordered (l_o), cholesterol-enriched raft domains as compared with the lipid-disordered (l_d) domains in DOPC/DPPC bilayers (70). As a result, there is a significant strain on the boundary between the l_o and l_d domains, and therefore this region is more vulnerable to membrane-disrupting agents. An increase in cholesterol from 20 to 40 mol % increased the amount of dye that leaked from the DOPC/DPPC LUVs (Fig. 1 *B*) because the length of the boundary region was longer at the higher cholesterol concentration. This observation is in agreement with recent reports that lipid bilayers containing cholesterol-enriched raft domains were easily disrupted by cationic antimicrobial peptides such as pexiganan (also known as MSI-78) (71,72).

DOPC/DPPC membranes contain raft-like domains

The flat morphology of the SLBs of DOPC/DPPC (1:2) in the absence of IAPP is shown in Fig. 2 *A*. Multistacks of SLBs without any segregation are observed. When 20% cholesterol was added, small defects appeared on the lipid bilayer surface, as shown in Fig. 2 *B*. Lipid rafts and multidomain rafts appeared when the cholesterol content was increased to 30% (Fig. 2 *C*) and 40% (Fig. 2 *D*), respectively. These findings are consistent with an atomistic description of the lipid systems obtained from MD simulations as shown in Figs. S1–S5 in the Supporting Material.

Next, to shed light on the observed IAPP-induced dye leakage from lipid vesicles, we acquired AFM micrographs of SLBs containing 0, 20, 30, and 40% cholesterol after 1 h of incubation with IAPP. Representative AFM micrographs of 1:2 DOPC/DPPC containing 30% cholesterol are shown in Fig. 3. Lipid rafts surrounding the edge of fibrils (Fig. 3 *A*), as well as broken SBLs and pores, are visible (Fig. 3 *D*). It is interesting to note that the system is highly dynamic, as evidenced by the images acquired after 5 min (Fig. 3 *D*) and 10 min (Fig. 3 *E*).

To observe the fiber-dependent effects on membrane integrity, we monitored IAPP fiber formation on SBLs containing 0, 20, 30, and 40% cholesterol after 6 h of incubation (Fig. 4). The AFM images shown in Fig. 4 reveal that an increasing amount of cholesterol decreased the amount of IAPP fibers and disruption of the SBLs.

In the absence of cholesterol (Fig. 4 *A*), broken SBLs could be observed (indicated as *b*) and the dimension of the fibrils was ~10–15 nm. The sample containing 20% cholesterol (Fig. 4 *B*) shows the insertion of an IAPP fibril into a bilayer (indicated as *a*, ~10 nm in height) and fiber-interrupted SBLs (indicated as *b*). With 30% cholesterol, the higher amount of fibers (~15 nm in height) disrupted the

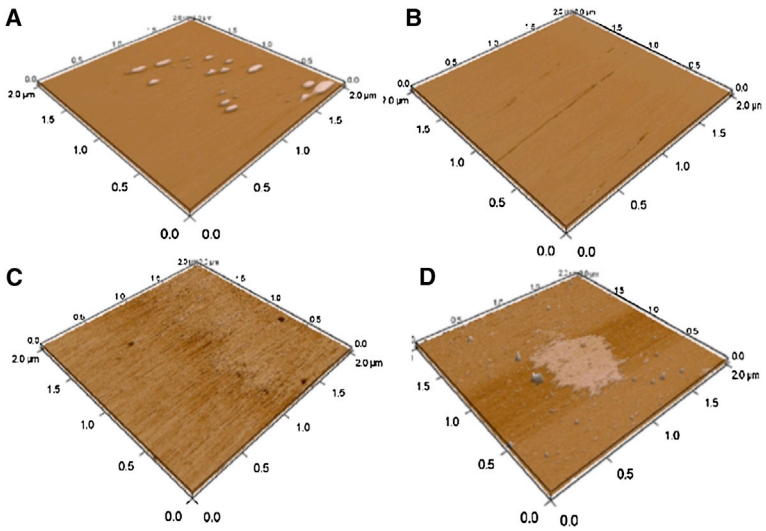

FIGURE 2 (*A–D*) AFM images of samples containing 1:2 DOPC/DPPC SLBs with 0% (*A*), 20% (*B*), 30% (*C*), and 40% (*D*) cholesterol. To see this figure in color, go online.

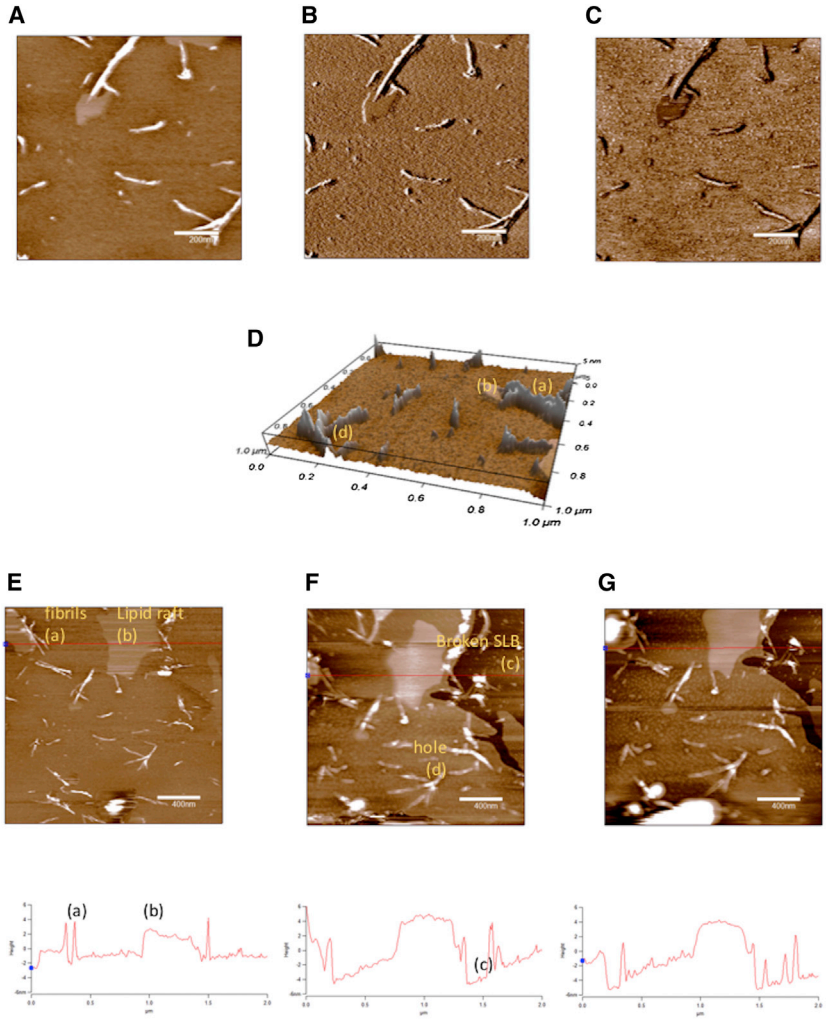

FIGURE 3 (*A–D*) AFM images at 1 μm^2 scan size of (*A*) height in two dimensions (z scale = 10 nm), (*B*) amplitude, (*C*) phase, and (*D*) height in three dimensions (z scale = 10 nm) of 1:2 DOPC/DPPC SLBs containing 30% cholesterol after 1 h of incubation with 10 μM IAPP. (*E–G*) Time-lapse images of height (4 μm^2 scan size; z scale = 15 nm) of samples containing 1:2 DOPC/DPPC SLBs and 30% cholesterol after (*E*) 1 h, (*F*) 65 min, and (*G*) 70 min of incubation with 10 μM IAPP. Features labeled as (*a*), (*b*), (*c*), and (*d*) refer to fibril, lipid raft, broken SLB, and holes in the lipid bilayer, respectively. To see this figure in color, go online.

SBLs, whereas samples containing 40% cholesterol showed fibrils and largely damaged SLBs.

Cholesterol does not alter the kinetics of IAPP fiber formation in raft-free POPC/POPS bilayers

It is known that cholesterol exerts a significant ordering effect on the acyl chains of phosphatidylserine-rich, fluid lipid bilayers, with consequent changes in their propensity to interact with amyloid-forming peptides (73,74). Thus, we employed ThT assays to investigate IAPP fiber growth kinetics in the presence of POPC/POPS (7:3 molar ratio) LUVs containing increasing amounts of cholesterol. The results (Fig. 5 *A*) show that the cholesterol concentration did not significantly influence the kinetics of fiber formation, which occurred in ~300 min for all samples, in agreement with data reported in the literature (67).

However, cholesterol enhanced the fiber elongation rate and the total amount of fibers that formed. This result is consistent with previous reports showing that cholesterol is deeply embedded in the hydrophobic core of the lipid bilayer (75,76) and therefore does not modify the properties of the membrane surface. Otherwise, any significant change in the negative charge density on the LUVs should have significantly influenced the kinetics of fiber formation, as suggested in the literature (77).

Cholesterol suppresses pore formation and enhances fiber-dependent POPC/POPS bilayer disruption by IAPP

Fig. 5 *B* illustrates the IAPP-induced disruption of 7:3 molar ratio POPC/POPS LUVs. The experimental results reveal a two-step membrane-disruption process, as reported in a previous study (67). The membrane interaction with IAPP induces significant dye leakage even in the lag phase (0–300 min in Fig. 1 *B*, *black trace*), i.e., before the formation of amyloid fibers (first step). Then, in the second step ($t > 300$ min in Fig. 1 *B*), the fiber formation induces increasing dye leakage that reaches a maximum after 400 min, thus paralleling the ThT fluorescence results shown in Fig. 5 *A*. Interestingly, the presence of cholesterol

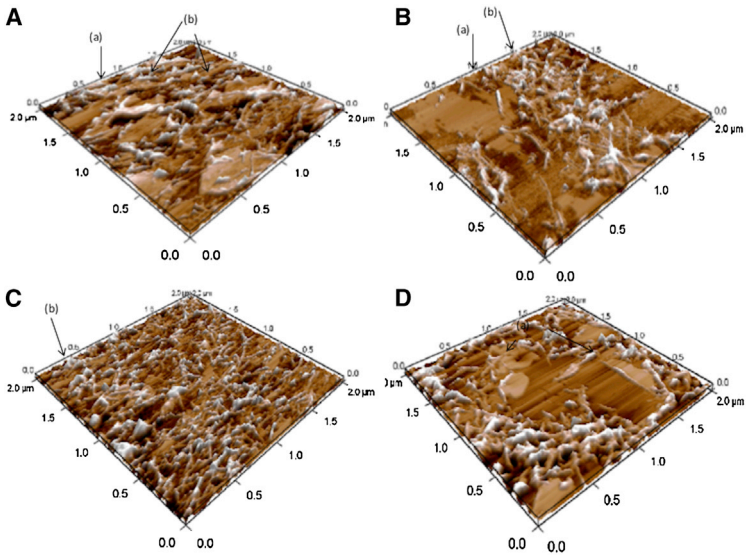

FIGURE 4 (*A–D*) AFM images of 1:2 DOPC/DPPC SLBs after 6 h of incubation with 10 μM IAPP: (*A*) 0%, (*B*) 20%, (*C*) 30%, and (*D*) 40% cholesterol. To see this figure in color, go online.

inhibits the first (pore-forming) step of the IAPP-induced membrane disruption, whereas the step associated with fiber elongation is enhanced by cholesterol in a dose-dependent way. This behavior is likely due to a cholesterol-induced increase in the lateral pressure of the lipid bilayers, as noted above (78). Thus, cholesterol enhances the order of lipid acyl chains, resulting in a rigidifying effect on the membranes, with a concomitant inhibition of IAPP insertion into the lipid bilayers to form pores. As a result, this effect enhances the propensity to disrupt membranes through a detergent-like mechanism induced by the growth of fibers on the membrane surface (79). Indeed, as shown in Fig. 5 *B*, the presence of cholesterol reduces the lag time of IAPP fiber formation and increases the amount of dye that is released upon IAPP-mediated membrane disruption.

Cholesterol suppresses the coil-to-helix transition of IAPP in POPC/POPS bilayers

The structural features of IAPP have a great influence on its membrane-damaging potential, and therefore it is important to capture membrane-bound IAPP conformations. To address this issue, we performed CD experiments by titrating a freshly prepared solution of IAPP with 7:3 POPC/POPS LUVs (Fig. 6).

The interaction of IAPP with the membrane surface was previously shown to result in an increase of α-helical structure (77,80). As shown in Fig. 6 *B*, IAPP exhibits a random-coil structure in buffer and transitions to a helical structure upon its interaction with POPC/POPS LUVs. Thus, the changes in molar ellipticity observed at 222 nm can provide a quantitative estimate of the interaction of IAPP with the membrane surface (67). The experimental results shown in Fig. 6 *A* suggest that the extent of the random-coil-to-helix transition of IAPP is decreased with increasing amounts of cholesterol. Although the addition of 20 mol % cholesterol to POPC/POPS LUVs significantly reduced the extent of the helical structure of IAPP, an increase in the cholesterol concentration to 30 mol % and beyond significantly suppressed the coil-to-helical-structure transition of IAPP (Fig. 6 *B*). These observations suggest that the presence of cholesterol rigidifies the acyl chains of lipids and therefore inhibits the insertion of IAPP into lipid bilayers, which is in excellent agreement with the dye-leakage data showing an inhibition of pore formation (Fig. 5). These results are also in agreement with previous NMR studies that showed that the N-terminal region of IAPP forms a transmembrane helix in membranes in the absence of cholesterol to enable pore formation, which is the first step of the membrane-disruption process (16,81). In addition, it is likely that the presence of cholesterol in the hydrophobic core of the POPC/POPS bilayer also exerts a rigidifying effect on the membrane surface, which forces the peptide to aggregate instead of allowing it to form a helix as observed for $\geq$30% cholesterol (Fig. 6). This interpretation is also in agreement with the increased dye leakage in the second step of the membrane-disruption process, as shown in Fig. 3. The random-coil-to-α-helix transition was not clearly observed in the presence of 1:2 DOPC/DPPC LUVs (Fig. 6 *C*). In this case, we observed an increase in the β-sheet content that was proportional to the percentage of cholesterol. All samples exhibited a β-sheet conformation after 24 h of incubation (data not shown).

AFM reveals prefibrillar and fibrillar IAPP aggregates on the surface of POPC/POPS bilayers

It is known that the morphology of IAPP assemblies may significantly affect their ability to interact with membrane. To shed light on this process, we obtained AFM images of samples containing IAPP in the presence of 7:3 POPC/POPS SLBs at different cholesterol concentrations (Fig. 7)

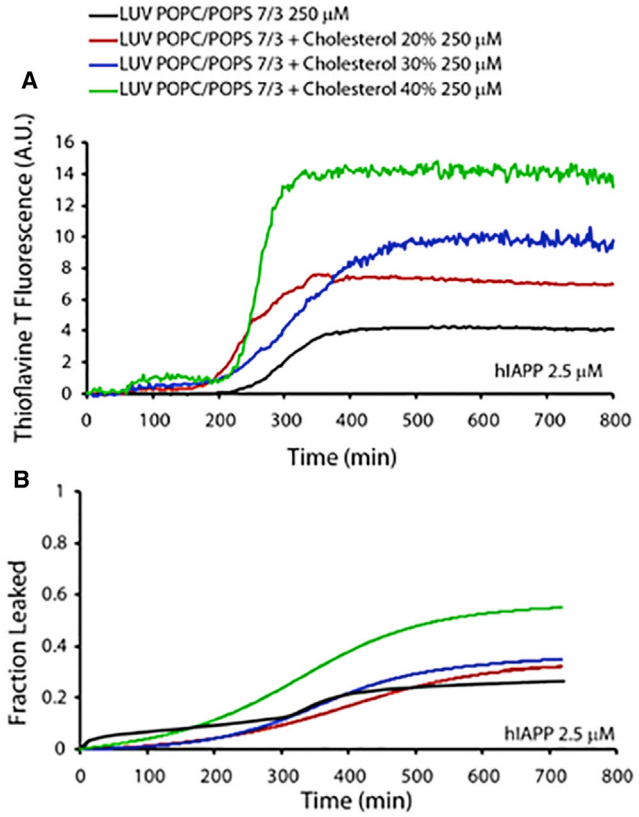

FIGURE 5 IAPP fiber-formation kinetics and membrane disruption in the presence of POPC/POPS LUVs. (*A*) ThT fluorescence showing IAPP amyloid fiber formation was measured in the presence of 250 μM POPC/POPS (7:3 molar ratio) LUVs, pure containing 0% (*black curve*) or containing 20% (*red curve*), 30% (*blue curve*), or 40% (*green curve*) cholesterol. The IAPP concentration was 2.5 μM for all samples. (*B*) Fraction of carboxyfluorescein dye that leaked from 250 μM (7:3 molar ratio) POPC/POPS LUVs due to membrane disruption induced by IAPP. Release of 6-carboxyfluorescein from LUVs composed of 250 μM POPC/POPS (7:3 molar ratio), pure containing 0% (*black curve*) or containing 20% (*red curve*), 30% (*blue curve*), or 40% (*green curve*) cholesterol, induced by 2.5 μM IAPP. The IAPP concentration was 2.5 μM for all samples. All experiments were performed at 25°C in 10 mM phosphate buffer with 100 mM NaCl, pH 7.4. Results are the average of three experiments. To see this figure in color, go online.

after 700 min of incubation. The AFM images show amyloid fibers interacting with the lipid membrane surface, whereas fibrils that formed in solution are eliminated during sample preparation. It is evident that the amount of fibers on the surface of SLBs increases with the cholesterol content, in accordance with the dye-leakage results. Globular structures observed in samples with low concentrations of cholesterol (Fig. 7 *A*) are probably small-sized IAPP aggregates deposited on the surface of the bilayer.

The presence of cholesterol increases the number of domains and decreases their size in DOPC/DPPC membranes

Our experimental data indicate that IAPP exhibits different behaviors when it interacts with different micro-structured model membranes with and without rafts. Raft-containing membranes inhibit the lag phase and increase the kinetics of fibril formation, enhance pore-like structures, and change the fibril morphology as compared with membranes that contain no rafts. To further describe these two types of lipid bilayers at a molecular level, we performed all-atom MD simulations on DOPC/DPPC/Chol bilayers. Fig. 8 shows the positions of DOPC, DPPC, and cholesterol in a bilayer obtained during the last 150 ns of 300 ns MD simulations, and Fig. 9 shows the corresponding bilayer thickness profile obtained with increasing cholesterol contents.

Different domains containing DPPC (*red*) and DOPC (*blue*) appear in the absence of cholesterol (Fig. 8 *A*). As expected, the DPPC domains are thicker (~50 Å) than the DOPC domains (~38 Å), as reported in Fig. 9.

By increasing the amount of cholesterol (Fig. 8, *green*) up to 30 mol %, we observed an increase in the number of domains but a decrease in the domain size (Fig. 8). The large lipidic domain seemed to disappear in a sample with 40 mol % of cholesterol (Fig. 8 *D*), and a flat thickness profile was observed (Fig. 9 *D*). Notably, according to a previous experimental report (82), cholesterol essentially is more soluble in a high-melting-temperature lipid (DPPC) and at a high concentration forms domains by locating itself in the hydrocarbon core (Fig. S1) at the borderline of the DPPC and DOPC domains. To gain quantitative insight into the cholesterol interaction with lipid hydrocarbon chain, we evaluated the order parameter S_{CD} and radial distribution function $g(r)$.

Order parameters for the four systems were calculated to quantify the grade of order/disorder of lipids (Fig. S1). S_{CD} increases with an increasing cholesterol percentage: its value tends to be 0.5 when C_i is parallel to the z axis of the lipid bilayer. This evidence is consistent with previous data (83–86) obtained from NMR experiments and simulations that showed that cholesterol preferentially interacts with the border of DPPC instead of exhibiting a random distribution, and the size of DPPC domains decreases with increasing cholesterol concentration.

We evaluated the radial distribution function to understand the degree of order of DPPC molecules in the bilayer and how cholesterol perturbs this order (Fig. S2). We calculated the radial distribution function by considering the DPPC-DPPC distance and carbon atom C8 of the *sn* 2 hydrocarbon chain. The data obtained show a long-range order for DPPC in the absence of cholesterol. This long-range order is lost when cholesterol reaches a concentration of $\geq$30%. This finding is an index of the decrease in the DPPC cluster size with increasing cholesterol concentration.

The diffusivity constant (K) (87) and area/molecule (A) of DOPC/DPPC (1:2) at different cholesterol contents are shown in Table 1. In agreement with a previous study (88), the DOPC/DPPC mixture has K and A values typical

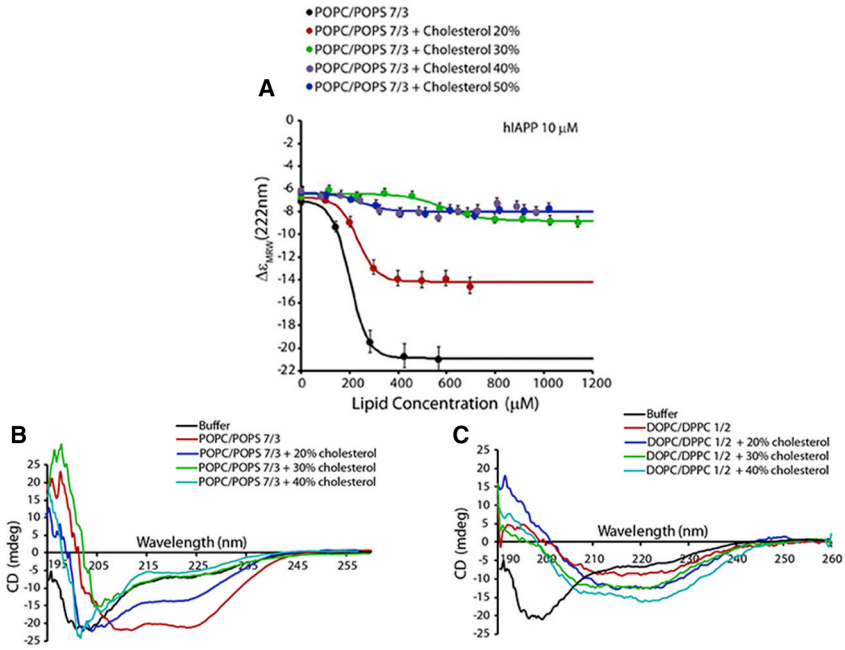

FIGURE 6 Binding of prefibrillar IAPP to POPC/POPS LUVs. (*A*) Changes in molar ellipticity at 222 nm arising from a coil-to-helix conformational change upon membrane binding as a function of lipid concentration. Freshly dissolved IAPP (10 μM) was titrated with the indicated concentrations of 7:3 POPC/POPS LUVs containing 0 mol % (*black*), 20% (*red*), 30% (*green*), 40% (*gray*), or 50% (*blue*) cholesterol. Experiments were performed at 25°C in 10 mM phosphate buffer with 100 mM NaF, pH 7.4. Results are the average of three experiments. (*B* and *C*) CD spectra of IAPP in the presence of 200 μM LUVs of 7:3 POPC/POPS (*B*) and 1:2 DOPC/DPPC (*C*) containing varying amounts of cholesterol. To see this figure in color, go online.

of the l_o phase and these values remain constant, within statistical uncertainty, with increasing percentages of cholesterol.

DISCUSSION

Previous studies have shown that the lipid membrane interaction with IAPP plays a very important role in islet cell toxicity and T2DM (17,89). However, the role played by cholesterol in the development of amyloid disease is unclear, as several studies reported conflicting results indicating that cholesterol may either protect membranes against amyloid-mediated permeabilization or affect the membrane integrity (90,91). In particular, although many evidences point to cholesterol as a causative agent of T2DM, its exact role in IAPP-evoked membrane damage and fibrillogenesis is still under debate (92). Previous experiments have demonstrated that IAPP aggregates in the presence of 1:2:1 DPPC/DOPC/Chol (model raft-containing membranes), but not in pure DOPC bilayers (93). In

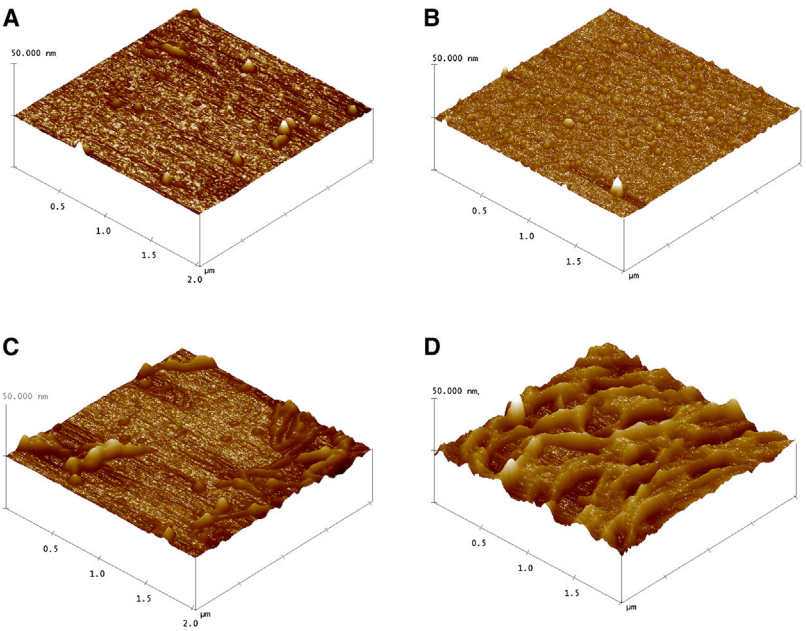

FIGURE 7 (*A–D*) AFM images of POPC/POPS SLB (7:3 molar ratio) samples containing 10 μM IAPP with 0% (*A*), 20% (*B*), 30% (*C*), or 40% (*D*) cholesterol. To see this figure in color, go online.

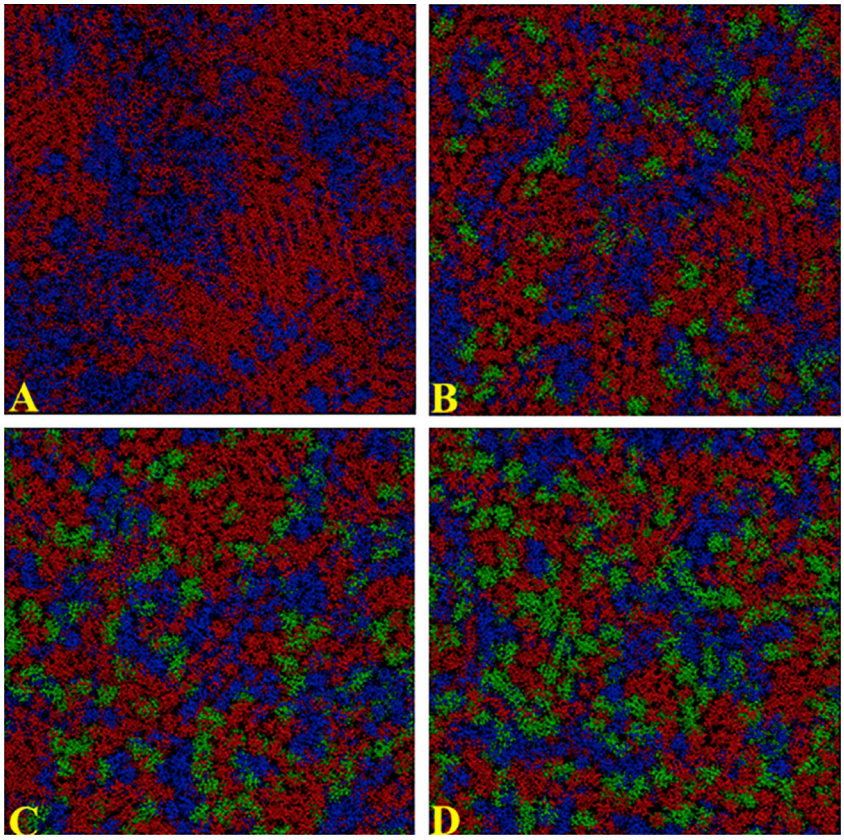

FIGURE 8 (*A–D*) CPK representations of a phospholipid bilayer containing a 1:2 molar ratio of DOPC/DPPC, averaged after 150 ns of atomistic MD simulations with the following contents of cholesterol: (*A*) 0%, (*B*) 20%, (*C*) 30%, and (*D*) 40%. Blue, DOPC; red, DPPC; green, cholesterol. To see this figure in color, go online.

contrast, pure POPC membrane is damaged in the presence of IAPP (94), and more recent CD and ThT fluorescence experiments have shown that zwitterionic lipid vesicles containing 30% cholesterol (7:3 DOPC/Chol) may inhibit IAPP fibril aggregation (95). In this study, we investigated the IAPP-membrane interaction using two different model lipid membrane systems: 7:3 POPC/POPS and raft-forming 1:2 DOPC/DPPC LUVs. Here, we show that an increased amount of cholesterol in 7:3 POPC/POPS model membranes has a negligible effect on the kinetics of IAPP fibril growth, whereas it inhibits pore formation and increases the detergent-like mechanism. In contrast, cholesterol significantly enhances both fiber (with significantly reduced lag time) and pore formation in raft-containing 1:2 DOPC/DPPC membranes. Moreover, the protein aggregate morphology

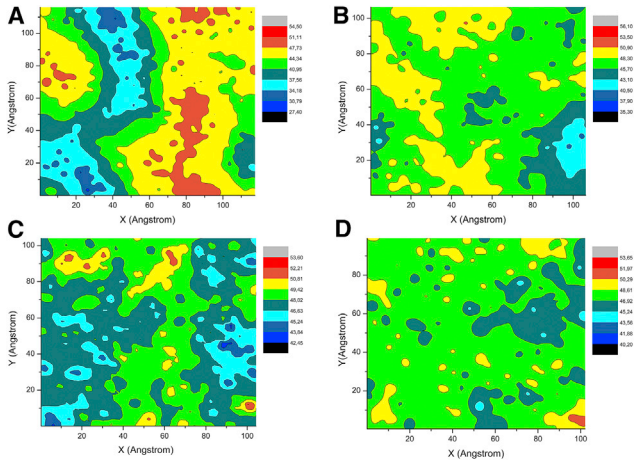

FIGURE 9 (*a–d*) Projection of a thickness profile in the *xy* plane of a phospholipid bilayer containing a 1:2 molar ratio of DOPC/DPPC, averaged after 150 ns of atomistic MD simulations with the following contents of cholesterol: (*a*) 0%, (*b*) 20%, (*c*) 30%, and (*d*) 40%. The thickness profile was evaluated by considering the average phosphorus-to-phosphorus distance. To see this figure in color, go online.

TABLE 1 Diffusivity and Area of Molecules in 1:2 DOPC:DPPC Raft Membranes Containing Various Amounts of Cholesterol Over the Last 150 ns of Simulation

Membrane Composition	DOPC		DPPC		Cholesterol	
DOPC/DPPC	*K*	*A*	*K*	*A*	*K*	*A*
0% cholesterol	27 (4)	55 (3)	20 (10)	48 (2)	–	–
20% cholesterol	11 (9)	55 (2)	10 (30)	48 (3)	9 (11)	31 (2)
30% cholesterol	11 (64)	47 (3)	7 (29)	46 (2)	8 (25)	27 (1)
40% cholesterol	13 (31)	47 (2)	10 (50)	46 (3)	9 (56)	27 (1)

Diffusivity $K \times 10^4$ (m^2/s) and area per molecule A ($Å^2$/molecule) of DOPC/DPPC (1:2) raft membranes with different cholesterol contents during the last 150 ns of simulation. Statistical uncertainty is expressed as a percentage in parentheses. *K* and *A* are given in the units of m^2/s and in $Å^2$/molecule, respectively. Statistical uncertainty is expressed as percentage in parenthesis.

is strongly influenced by the presence of rafts in the membrane, as revealed by AFM results.

Therefore, we can conclude that IAPP-mediated membrane leakage is modulated by cholesterol through its effects on the membrane's physicochemical properties. In a recent study, Krause et al. (96) addressed these issues by using the nearest-neighbor recognition methodology. Specifically, the authors proposed a push-pull mechanism in which interactions of cholesterol with unsaturated phospholipid chains are characterized by repulsive (push) or attractive (pull) forces. Our simulation data (Fig. 7) resemble the push-pull mechanism, since cholesterol accumulates preferentially near DPPC. We also show that cholesterol has a tendency to form aggregates with a linear morphology (most evident in a sample containing 40% cholesterol) and is mainly located at the boundary of the DPPC and DOPC domains (Fig. 7 *D*). Moreover, cholesterol contained within the DOPC/DOPS bilayer is randomly distributed, as observed elsewhere (97).

Our simulations reveal that raft-containing membranes are characterized by very different thicknesses and acyl-chain order parameters. The DOPC domain is characterized by a low thickness, low acyl-chain order parameter, and high area/molecule. In comparison, DPPC domains have a higher thickness, higher order parameter, and smaller area/molecule. This characteristic of raft membranes is seen in a surface view where the segregation of different lipid domains is evident. In contrast, a membrane without rafts (DOPC/DOPS) exhibits a homogeneous surface with lipids and cholesterol randomly distributed (Fig. S4).

A comparison of the MD and AFM results suggests that the membrane architecture may act as switch between pore formation and the detergent-like mechanism of IAPP. In particular, the small DOPC domains with a low thickness and order parameter and large area/lipid (the so-called l_d phase) show morphological features that are supposed to favor pore-forming protein aggregates. In contrast, the large lipid domains of DPPC with a high thickness and order parameter and small area/lipid (the l_o phase) do not favor a host-IAPP interaction and aggregate formation.

In conclusion, it is conceivable that the effect of cholesterol on IAPP penetration into membranes depends on a delicate equilibrium among 1) peptide-membrane electrostatic interactions, 2) a better match of the peptide hydrophobic domain with the bilayer thickness, and 3) the rigidifying effect of cholesterol on the lipid bilayer. Thus, it is likely that in 7:3 POPC/POPS bilayers the rigidifying effect of cholesterol prevails, which results in the inhibition of IAPP membrane binding and disruption. By contrast, hydrophobic effects likely dominate in raft-containing membranes, where cholesterol promotes IAPP-membrane interactions. The balance of all these forces is strictly dependent on the lipid composition, and thus it is not surprising that many studies have reported a variety of effects of cholesterol on different model membranes.

SUPPORTING MATERIAL

Five figures are available at http://www.biophysj.org/biophysj/supplemental/S0006-3495(16)30397-6.

AUTHOR CONTRIBUTIONS

M.F.M.S., G.D.M., C.S., and L.D. performed experiments; F.L. performed simulations; M.F.M.S., G.D.M., D.M., L.D., A.R., and C.L.R. analyzed the data; M.F.M.S., D.M., A.R., and C.L.R. designed the research and wrote the paper; and A.R. and C.L.R. directed the project.

ACKNOWLEDGMENTS

This study was partly supported by funds from the Protein Folding Disease Center at the University of Michigan and Hans Fischer Senior Fellowship from the Marie Curie COFUND program.

REFERENCES

1. Shai, I., D. Schwarzfuchs, …, M. J. Stampfer; Dietary Intervention Randomized Controlled Trial (DIRECT) Group. 2008. Weight loss with a low-carbohydrate, Mediterranean, or low-fat diet. *N. Engl. J. Med.* 359:229–241.
2. Unger, R. H. 1995. Lipotoxicity in the pathogenesis of obesity-dependent NIDDM. Genetic and clinical implications. *Diabetes.* 44:863–870.
3. Yaney, G. C., and B. E. Corkey. 2003. Fatty acid metabolism and insulin secretion in pancreatic beta cells. *Diabetologia.* 46:1297–1312.
4. Hao, M., W. S. Head, …, D. W. Piston. 2007. Direct effect of cholesterol on insulin secretion: a novel mechanism for pancreatic β-cell dysfunction. *Diabetes.* 56:2328–2338.
5. Tajima, R., S. Kodama, …, H. Sone. 2014. High cholesterol intake is associated with elevated risk of type 2 diabetes mellitus—a meta-analysis. *Clin. Nutr.* 33:946–950.
6. Sacks, F. M., M. P. Hermans, …, V. J. Carey. 2014. Association between plasma triglycerides and high-density lipoprotein cholesterol and microvascular kidney disease and retinopathy in type 2 diabetes mellitus: a global case-control study in 13 countries. *Circulation.* 129:999–1008.
7. Warnock, D. E., C. Roberts, …, J. U. Baenziger. 1993. Determination of plasma membrane lipid mass and composition in cultured Chinese hamster ovary cells using high gradient magnetic affinity chromatography. *J. Biol. Chem.* 268:10145–10153.
8. Hao, M., S. X. Lin, …, F. R. Maxfield. 2002. Vesicular and nonvesicular sterol transport in living cells. The endocytic recycling compartment is a major sterol storage organelle. *J. Biol. Chem.* 277:609–617.
9. Le Lay, S., S. Krief, …, I. Dugail. 2001. Cholesterol, a cell size-dependent signal that regulates glucose metabolism and gene expression in adipocytes. *J. Biol. Chem.* 276:16904–16910.
10. Brown, M. S., and J. L. Goldstein. 1997. The SREBP pathway: regulation of cholesterol metabolism by proteolysis of a membrane-bound transcription factor. *Cell.* 89:331–340.
11. Simons, K., and E. Ikonen. 1997. Functional rafts in cell membranes. *Nature.* 387:569–572.
12. Westermark, P., A. Andersson, and G. T. Westermark. 2011. Islet amyloid polypeptide, islet amyloid, and diabetes mellitus. *Physiol. Rev.* 91:795–826.

13. Lacy, P. E. 1967. The pancreatic beta cell. Structure and function. *N. Engl. J. Med.* 276:187–195.
14. Kayed, R., J. Bernhagen, …, A. Kapurniotu. 1999. Conformational transitions of islet amyloid polypeptide (IAPP) in amyloid formation in vitro. *J. Mol. Biol.* 287:781–796.
15. Knight, J. D., J. A. Hebda, and A. D. Miranker. 2006. Conserved and cooperative assembly of membrane-bound alpha-helical states of islet amyloid polypeptide. *Biochemistry.* 45:9496–9508.
16. Nanga, R. P. R., J. R. Brender, …, A. Ramamoorthy. 2009. Three-dimensional structure and orientation of rat islet amyloid polypeptide protein in a membrane environment by solution NMR spectroscopy. *J. Am. Chem. Soc.* 131:8252–8261.
17. Patil, S. M., S. Xu, …, A. T. Alexandrescu. 2009. Dynamic alpha-helix structure of micelle-bound human amylin. *J. Biol. Chem.* 284:11982–11991.
18. Williamson, J. A., and A. D. Miranker. 2007. Direct detection of transient α-helical states in islet amyloid polypeptide. *Protein Sci.* 16:110–117.
19. Milardi, D., M. Pappalardo, …, C. La Rosa. 2008. The role of the Cys2-Cys7 disulfide bridge in the early steps of islet amyloid polypeptide aggregation: a molecular dynamics study. *Chem. Phys. Lett.* 463:396–399.
20. Abedini, A., and D. P. Raleigh. 2009. A role for helical intermediates in amyloid formation by natively unfolded polypeptides? *Phys. Biol.* 6:015005.
21. Ramamoorthy, A., D.-K. Lee, …, R. P. R. Nanga. 2010. Cholesterol reduces pardaxin's dynamics—a barrel-stave mechanism of membrane disruption investigated by solid-state NMR. *Biochim. Biophys. Acta.* 1798:223–227.
22. Bell, E. T. 1952. Hyalinization of the islet of Langerhans in diabetes mellitus. *Diabetes.* 1:341–344.
23. Clark, A., C. A. Wells, …, R. C. Turner. 1988. Islet amyloid, increased A-cells, reduced B-cells and exocrine fibrosis: quantitative changes in the pancreas in type 2 diabetes. *Diabetes Res.* 9:151–159.
24. Ehrlich, J. C., and I. M. Ratner. 1961. Amyloidosis of the islets of Langerhans. A restudy of islet hyalin in diabetic and non-diabetic individuals. *Am. J. Pathol.* 38:49–59.
25. Westermark, P. 1972. Quantitative studies on amyloid in the islets of Langerhans. *Ups. J. Med. Sci.* 77:91–94.
26. Bell, E. T. 1959. Hyalinization of the islets of Langerhans in nondiabetic individuals. *Am. J. Pathol.* 35:801–805.
27. Lorenzo, A., and B. A. Yankner. 1996. Amyloid fibril toxicity in Alzheimer's disease and diabetes. *Ann. N. Y. Acad. Sci.* 777:89–95.
28. Janson, J., R. H. Ashley, …, P. C. Butler. 1999. The mechanism of islet amyloid polypeptide toxicity is membrane disruption by intermediate-sized toxic amyloid particles. *Diabetes.* 48:491–498.
29. Milardi, D., M. F. M. Sciacca, …, C. La Rosa. 2011. The role of aromatic side-chains in amyloid growth and membrane interaction of the islet amyloid polypeptide fragment LANFLVH. *Eur. Biophys. J.* 40:1–12.
30. Sciacca, M. F. M., M. Pappalardo, …, D. M. Grasso. 2010. Are fibril growth and membrane damage linked processes? An experimental and computational study of $IAPP_{12-18}$ and $IAPP_{21-27}$ peptides. *New J. Chem.* 34:200–207.
31. Lashuel, H. A., D. Hartley, …, P. T. Lansbury, Jr. 2002. Neurodegenerative disease: amyloid pores from pathogenic mutations. *Nature.* 418:291.
32. Mirzabekov, T. A., M. C. Lin, and B. L. Kagan. 1996. Pore formation by the cytotoxic islet amyloid peptide amylin. *J. Biol. Chem.* 271:1988–1992.
33. Porat, Y., S. Kolusheva, …, E. Gazit. 2003. The human islet amyloid polypeptide forms transient membrane-active prefibrillar assemblies. *Biochemistry.* 42:10971–10977.
34. Pannuzzo, M., A. Raudino, …, M. Karttunen. 2013. α-Helical structures drive early stages of self-assembly of amyloidogenic amyloid polypeptide aggregate formation in membranes. *Sci. Rep.* 3:2781.
35. Sciacca, M. F., D. Milardi, …, C. La Rosa. 2013. Cations as switches of amyloid-mediated membrane disruption mechanisms: calcium and IAPP. *Biophys. J.* 104:173–184.
36. Smith, P. E. S., J. R. Brender, and A. Ramamoorthy. 2009. Induction of negative curvature as a mechanism of cell toxicity by amyloidogenic peptides: the case of islet amyloid polypeptide. *J. Am. Chem. Soc.* 131:4470–4478.
37. Kayed, R., Y. Sokolov, …, C. G. Glabe. 2004. Permeabilization of lipid bilayers is a common conformation-dependent activity of soluble amyloid oligomers in protein misfolding diseases. *J. Biol. Chem.* 279:46363–46366.
38. Sokolov, Y., J. A. Kozak, …, J. E. Hall. 2006. Soluble amyloid oligomers increase bilayer conductance by altering dielectric structure. *J. Gen. Physiol.* 128:637–647.
39. Engel, M. F. M., L. Khemtémourian, …, J. W. M. Höppener. 2008. Membrane damage by human islet amyloid polypeptide through fibril growth at the membrane. *Proc. Natl. Acad. Sci. USA.* 105:6033–6038.
40. Brender, J. R., E. L. Lee, …, A. Gafni. 2011. Biphasic effects of insulin on islet amyloid polypeptide membrane disruption. *Biophys. J.* 100:685–692.
41. Cho, W., B. P. Jena, and A. M. Jeremic. 2008. Nano-scale imaging and dynamics of amylin-membrane interactions and its implication in type II diabetes mellitus. *Methods Cell Biol.* 90:267–286.
42. Cho, W.-J., S. Trikha, and A. M. Jeremic. 2009. Cholesterol regulates assembly of human islet amyloid polypeptide on model membranes. *J. Mol. Biol.* 393:765–775.
43. Trikha, S., and A. M. Jeremic. 2011. Clustering and internalization of toxic amylin oligomers in pancreatic cells require plasma membrane cholesterol. *J. Biol. Chem.* 286:36086–36097.
44. Wakabayashi, M., and K. Matsuzaki. 2009. Ganglioside-induced amyloid formation by human islet amyloid polypeptide in lipid rafts. *FEBS Lett.* 583:2854–2858.
45. Chakravarthy, M. V., and C. F. Semenkovich. 2007. The ABCs of β-cell dysfunction in type 2 diabetes. *Nat. Med.* 13:241–242.
46. Brunham, L. R., J. K. Kruit, …, M. R. Hayden. 2007. Beta-cell ABCA1 influences insulin secretion, glucose homeostasis and response to thiazolidinedione treatment. *Nat. Med.* 13:340–347.
47. Xia, F., X. Gao, …, R. G. Tsushima. 2004. Disruption of pancreatic β-cell lipid rafts modifies Kv2.1 channel gating and insulin exocytosis. *J. Biol. Chem.* 279:24685–24691.
48. Gellermann, G. P., T. R. Appel, …, M. Fändrich. 2005. Raft lipids as common components of human extracellular amyloid fibrils. *Proc. Natl. Acad. Sci. USA.* 102:6297–6302.
49. Jo, S., T. Kim, and W. Im. 2007. Automated builder and database of protein/membrane complexes for molecular dynamics simulations. *PLoS One.* 2:e880.
50. Jo, S., T. Kim, …, W. Im. 2008. CHARMM-GUI: a web-based graphical user interface for CHARMM. *J. Comput. Chem.* 29:1859–1865.
51. Jo, S., J. B. Lim, …, W. Im. 2009. CHARMM-GUI Membrane Builder for mixed bilayers and its application to yeast membranes. *Biophys. J.* 97:50–58.
52. Yu, W., X. He, …, A. D. MacKerell, Jr. 2012. Extension of the CHARMM general force field to sulfonyl-containing compounds and its utility in biomolecular simulations. *J. Comput. Chem.* 33:2451–2468.
53. Vanommeslaeghe, K., E. Hatcher, …, A. D. Mackerell, Jr. 2010. CHARMM general force field: a force field for drug-like molecules compatible with the CHARMM all-atom additive biological force fields. *J. Comput. Chem.* 31:671–690.
54. Mahoney, M. W., and W. L. Jorgensen. 2000. A five-site model for liquid water and the reproduction of the density anomaly by rigid, nonpolarizable potential functions. *J. Chem. Phys.* 112:8910–8922.
55. Christopher, J. A., J. Brown, …, M. Congreve. 2013. Biophysical fragment screening of the β1-adrenergic receptor: identification of high affinity arylpiperazine leads using structure-based drug design. *J. Med. Chem.* 56:3446–3455.

56. Warne, T., R. Moukhametzianov, …, C. G. Tate. 2011. The structural basis for agonist and partial agonist action on a β(1)-adrenergic receptor. *Nature.* 469:241–244.

57. Parrinello, M., and A. Rahman. 1981. Polymorphic transitions in single crystals: a new molecular dynamics method. *J. Appl. Phys.* 52:7182–7190.

58. Nosé, S., and M. L. Klein. 1983. Constant pressure molecular dynamics for molecular systems. *Mol. Phys.* 50:1055–1076.

59. Brooks, B. R., C. L. Brooks, 3rd, …, M. Karplus. 2009. CHARMM: the biomolecular simulation program. *J. Comput. Chem.* 30:1545–1614.

60. Hess, B., H. Bekker, …, J. G. E. M. Fraaije. 1997. LINCS: a linear constraint solver for molecular simulations. *J. Comput. Chem.* 18:1463–1472.

61. Humphrey, W., A. Dalke, and K. Schulten. 1996. VMD: visual molecular dynamics. *J. Mol. Graph.* 14:33–38, 27–28.

62. Yonemoto, I. T., G. J. A. Kroon, …, J. W. Kelly. 2008. Amylin proprotein processing generates progressively more amyloidogenic peptides that initially sample the helical state. *Biochemistry.* 47:9900–9910.

63. Guixà-González, R., I. Rodriguez-Espigares, …, J. Selent. 2014. MEMBPLUGIN: studying membrane complexity in VMD. *Bioinformatics.* 30:1478–1480.

64. Di Natale, G., G. Pappalardo, …, E. Rizzarelli. 2010. Membrane interactions and conformational preferences of human and avian prion N-terminal tandem repeats: the role of copper(II) ions, pH, and membrane mimicking environments. *J. Phys. Chem. B.* 114:13830–13838.

65. Sciacca, M. F., M. Pappalardo, …, C. La Rosa. 2008. Calcium-activated membrane interaction of the islet amyloid polypeptide: implications in the pathogenesis of type II diabetes mellitus. *Arch. Biochem. Biophys.* 477:291–298.

66. Stewart, J. C. 1980. Colorimetric determination of phospholipids with ammonium ferrothiocyanate. *Anal. Biochem.* 104:10–14.

67. Sciacca, M. F. M., J. R. Brender, …, A. Ramamoorthy. 2012. Phosphatidylethanolamine enhances amyloid fiber-dependent membrane fragmentation. *Biochemistry.* 51:7676–7684.

68. Simons, K., and J. L. Sampaio. 2011. Membrane organization and lipid rafts. *Cold Spring Harb. Perspect. Biol.* 3:a004697.

69. Sciacca, M. F., S. A. Kotler, …, A. Ramamoorthy. 2012. Two-step mechanism of membrane disruption by Aβ through membrane fragmentation and pore formation. *Biophys. J.* 103:702–710.

70. Veatch, S. L., and S. L. Keller. 2002. Organization in lipid membranes containing cholesterol. *Phys. Rev. Lett.* 89:268101.

71. McHenry, A. J., M. F. Sciacca, …, A. Ramamoorthy. 2012. Does cholesterol suppress the antimicrobial peptide induced disruption of lipid raft containing membranes? *Biochim. Biophys. Acta.* 1818: 3019–3024.

72. Lee, D.-K., A. Bhunia, …, A. Ramamoorthy. 2015. Detergent-type membrane fragmentation by MSI-78, MSI-367, MSI-594, and MSI-843 antimicrobial peptides and inhibition by cholesterol: a solid-state nuclear magnetic resonance study. *Biochemistry.* 54:1897–1907.

73. Chong, P. L.-G., W. Zhu, and B. Venegas. 2009. On the lateral structure of model membranes containing cholesterol. *Biochim. Biophys. Acta.* 1788:2–11.

74. Epand, R. M., A. D. Bain, …, E. Wachtel. 2002. Properties of mixtures of cholesterol with phosphatidylcholine or with phosphatidylserine studied by (13)C magic angle spinning nuclear magnetic resonance. *Biophys. J.* 83:2053–2063.

75. Vijayan, R., and P. C. Biggin. 2008. A steroid in a lipid bilayer: localization, orientation, and energetics. *Biophys. J.* 95:L45–L47.

76. Mojumdar, E. H., D. Groen, …, J. A. Bouwstra. 2013. Localization of cholesterol and fatty acid in a model lipid membrane: a neutron diffraction approach. *Biophys. J.* 105:911–918.

77. Jayasinghe, S. A., and R. Langen. 2005. Lipid membranes modulate the structure of islet amyloid polypeptide. *Biochemistry.* 44:12113–12119.

78. Patra, M. 2005. Lateral pressure profiles in cholesterol-DPPC bilayers. *Eur. Biophys. J.* 35:79–88.

79. Marsh, D. 2007. Lateral pressure profile, spontaneous curvature frustration, and the incorporation and conformation of proteins in membranes. *Biophys. J.* 93:3884–3899.

80. Apostolidou, M., S. A. Jayasinghe, and R. Langen. 2008. Structure of α-helical membrane-bound human islet amyloid polypeptide and its implications for membrane-mediated misfolding. *J. Biol. Chem.* 283:17205–17210.

81. Nanga, R. P. R., J. R. Brender, …, A. Ramamoorthy. 2011. Structure and membrane orientation of IAPP in its natively amidated form at physiological pH in a membrane environment. *Biochim. Biophys. Acta.* 1808:2337–2342.

82. Marsh, D. 2009. Cholesterol-induced fluid membrane domains: a compendium of lipid-raft ternary phase diagrams. *Biochim. Biophys. Acta.* 1788:2114–2123.

83. Vermeer, L. S., B. L. de Groot, …, J. Czaplicki. 2007. Acyl chain order parameter profiles in phospholipid bilayers: computation from molecular dynamics simulations and comparison with 2H NMR experiments. *Eur. Biophys. J.* 36:919–931.

84. Risselada, H. J., and S. J. Marrink. 2008. The molecular face of lipid rafts in model membranes. *Proc. Natl. Acad. Sci. USA.* 105:17367–17372.

85. Petrache, H. I., K. Tu, and J. F. Nagle. 1999. Analysis of simulated NMR order parameters for lipid bilayer structure determination. *Biophys. J.* 76:2479–2487.

86. Braun, A. R., J. N. Sachs, and J. F. Nagle. 2013. Comparing simulations of lipid bilayers to scattering data: the GROMOS 43A1-S3 force field. *J. Phys. Chem. B.* 117:5065–5072.

87. Jeon, J.-H., H. M.-S. Monne, …, R. Metzler. 2012. Anomalous diffusion of phospholipids and cholesterols in a lipid bilayer and its origins. *Phys. Rev. Lett.* 109:188103.

88. Pyrkova, D. V., N. K. Tarasova, …, R. G. Efremov. 2011. Atomic-scale lateral heterogeneity and dynamics of two-component lipid bilayers composed of saturated and unsaturated phosphatidylcholines. *Soft Matter.* 7:2569–2579.

89. Brender, J. R., S. Salamekh, and A. Ramamoorthy. 2012. Membrane disruption and early events in the aggregation of the diabetes related peptide IAPP from a molecular perspective. *Acc. Chem. Res.* 45:454–462.

90. Pieri, L., M. Bucciantini, …, M. Stefani. 2009. Synthetic lipid vesicles recruit native-like aggregates and affect the aggregation process of the prion Ure2p: insights on vesicle permeabilization and charge selectivity. *Biophys. J.* 96:3319–3330.

91. Yu, X., and J. Zheng. 2012. Cholesterol promotes the interaction of Alzheimer β-amyloid monomer with lipid bilayer. *J. Mol. Biol.* 421:561–571.

92. Milardi, D., M. F. Sciacca, …, C. La Rosa. 2014. The role of calcium, lipid membranes and islet amyloid polypeptide in the onset of type 2 diabetes: innocent bystanders or partners in a crime? *Front. Endocrinol. (Lausanne).* 5:216.

93. Jha, S., D. Sellin, …, R. Winter. 2009. Amyloidogenic propensities and conformational properties of ProIAPP and IAPP in the presence of lipid bilayer membranes. *J. Mol. Biol.* 389:907–920.

94. Scalisi, S., M. F. M. Sciacca, …, C. La Rosa. 2010. Self-assembling pathway of HiApp fibrils within lipid bilayers. *ChemBioChem.* 11:1856–1859.

95. Caillon, L., O. Lequin, and L. Khemtémourian. 2013. Evaluation of membrane models and their composition for islet amyloid polypeptide-membrane aggregation. *Biochim. Biophys. Acta.* 1828:2091–2098.

96. Krause, M. R., T. A. Daly, …, S. L. Regen. 2014. Push-pull mechanism for lipid raft formation. *Langmuir.* 30:3285–3289.

97. Ge, M., A. Gidwani, …, J. H. Freed. 2003. Ordered and disordered phases coexist in plasma membrane vesicles of RBL-2H3 mast cells. An ESR study. *Biophys. J.* 85:1278–1288.

Biophysical Journal, Volume *111*

Supplemental Information

The Role of Cholesterol in Driving IAPP-Membrane Interactions

Michele F.M. Sciacca, Fabio Lolicato, Giacomo Di Mauro, Danilo Milardi, Luisa D'Urso, Cristina Satriano, Ayyalusamy Ramamoorthy, and Carmelo La Rosa

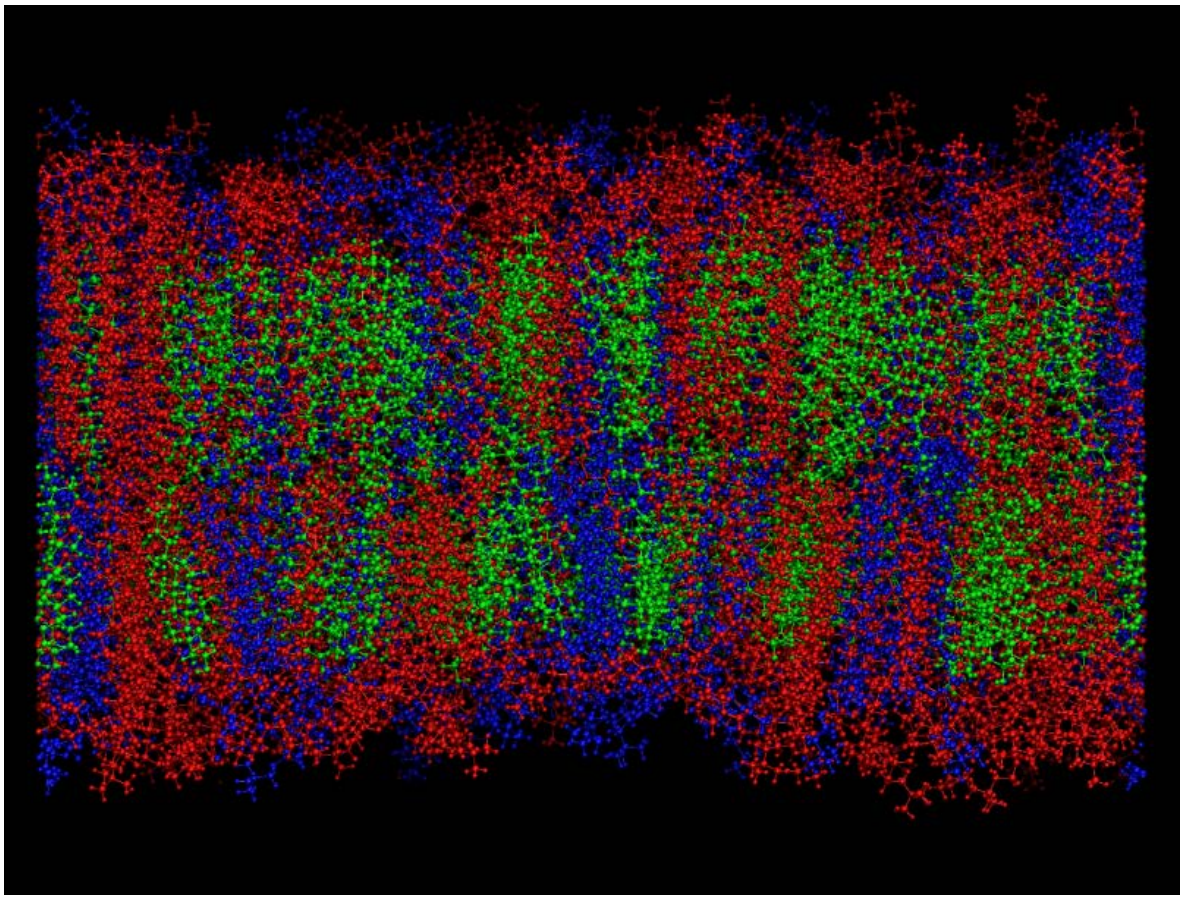

Figure S1. Location of cholesterol in a lipid bilayer obtained after 300 ns molecular dynamics simulation of DPPC/DOPC containing 40% of cholesterol.

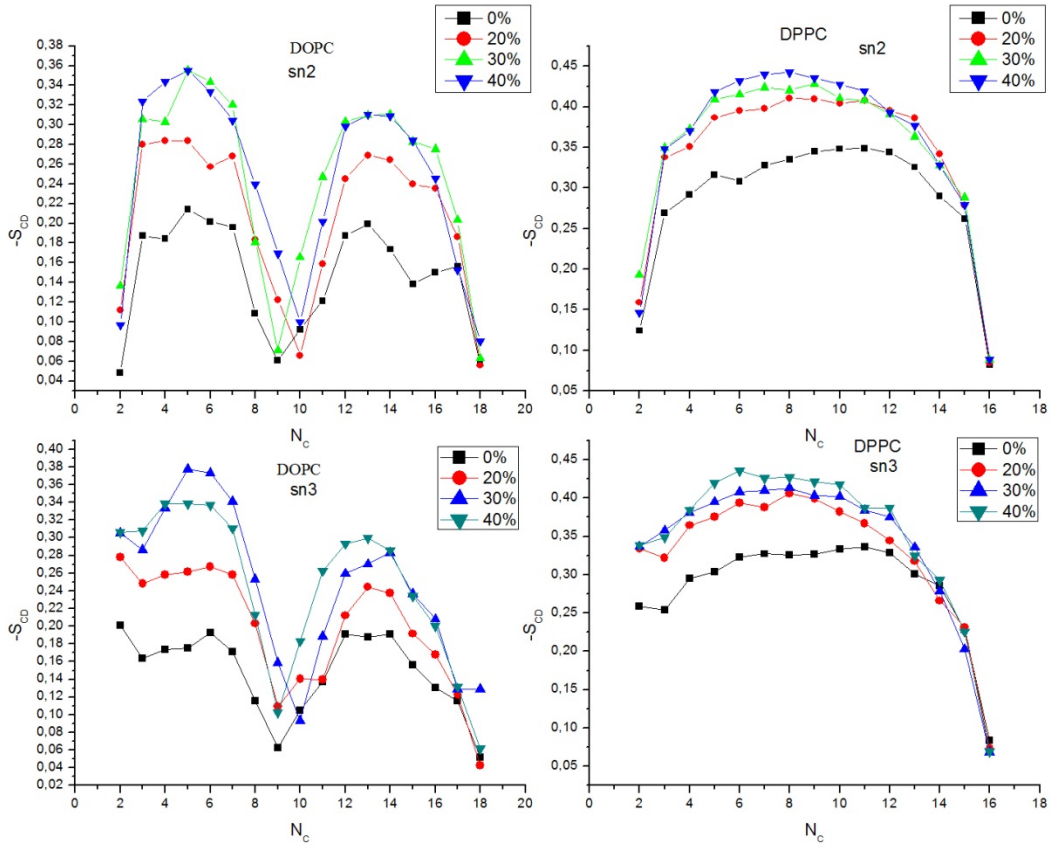

Figure S2. Order parameters ($-S_{CD}$) of DOPC/DPPC/Cholesterol lipid bilayers calculated from MD simulations. S_{CD} was evaluated as averagedover last 50 ns of simulations by takingboth leaflets into account. DOPC carbon-carbon double bond of sn2 (black) and sn3 (red) hydrocarbon chains are between C9-C10.

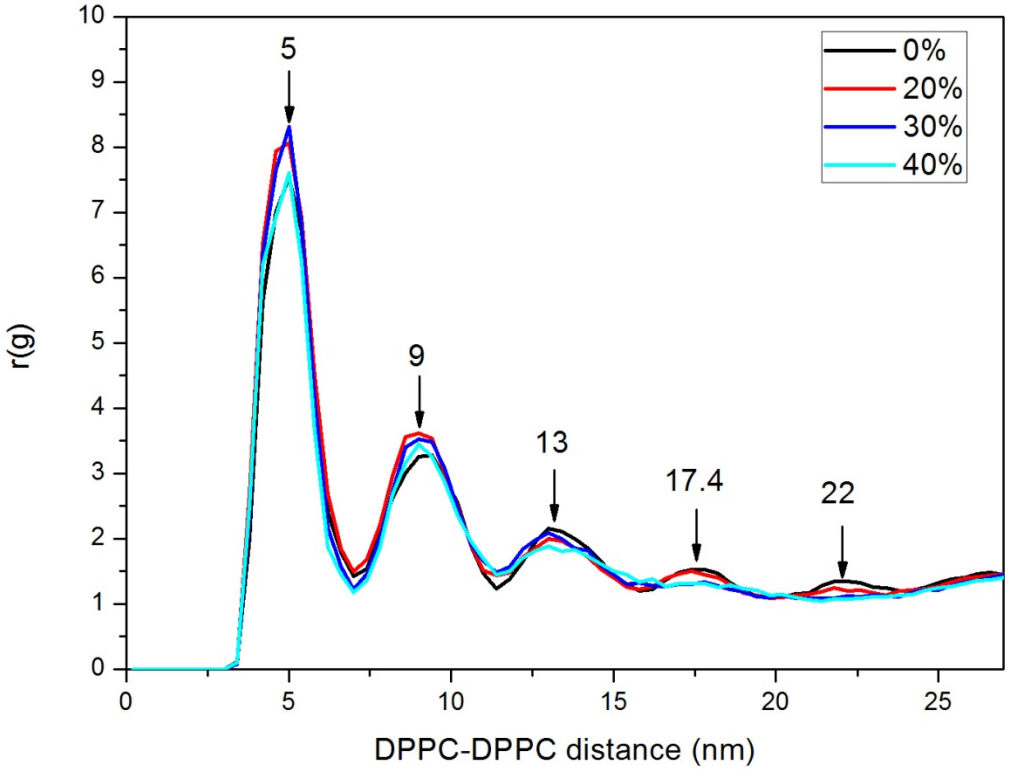

Figure S3. Radial distribution function of DPPC in mixture with DOPC and a varyingamount of cholesterol: 0% black; 20% red; 30% blue and 40% cyan. R(g) was calculated for C8 carbon atom of DPPC-DPPC.

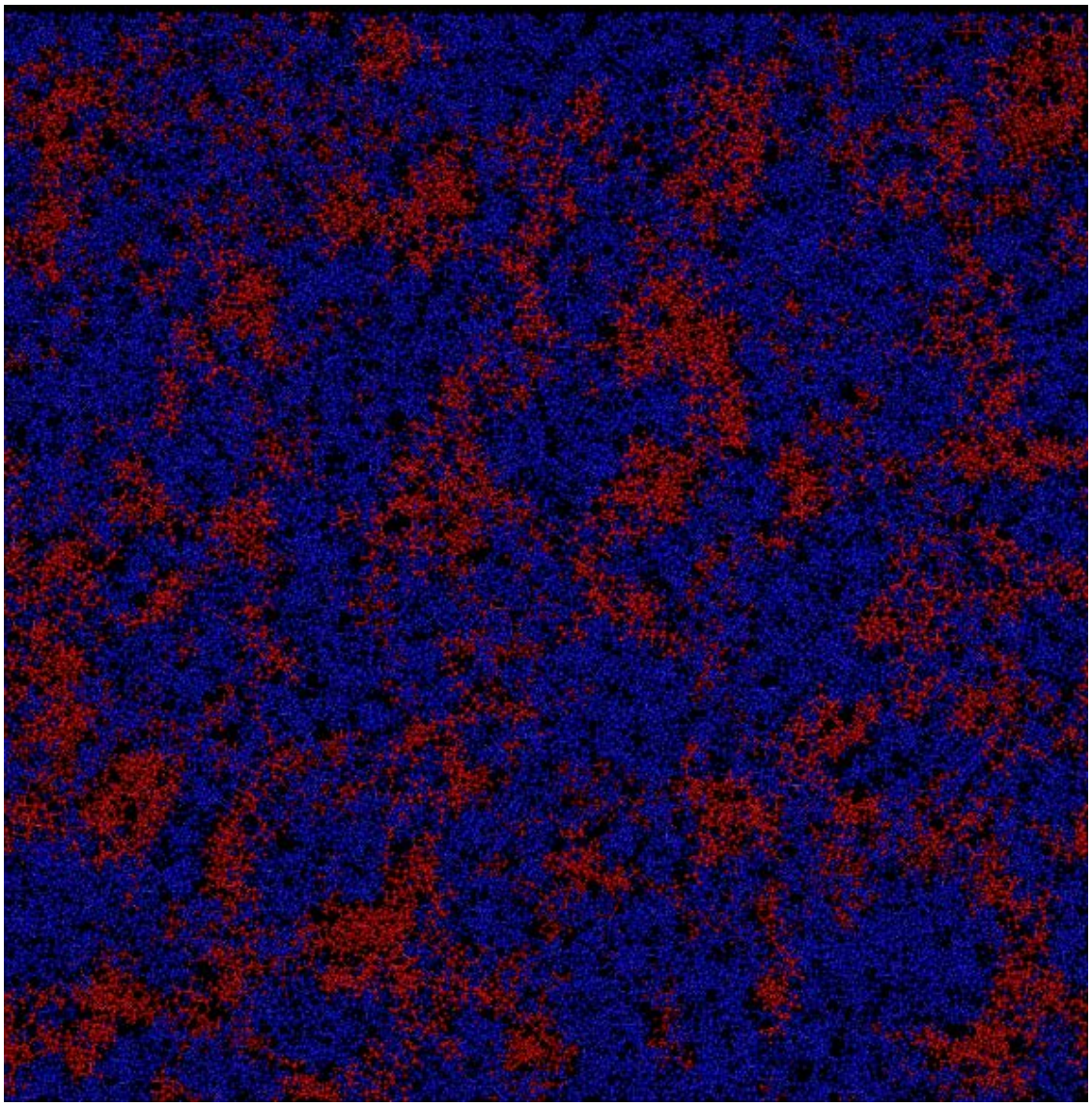

Figure S4. Top view of phospholipid distribution in aDOPC:DOPS (7:3) lipid bilayers after 300 ns of molecular dynamic simulations.

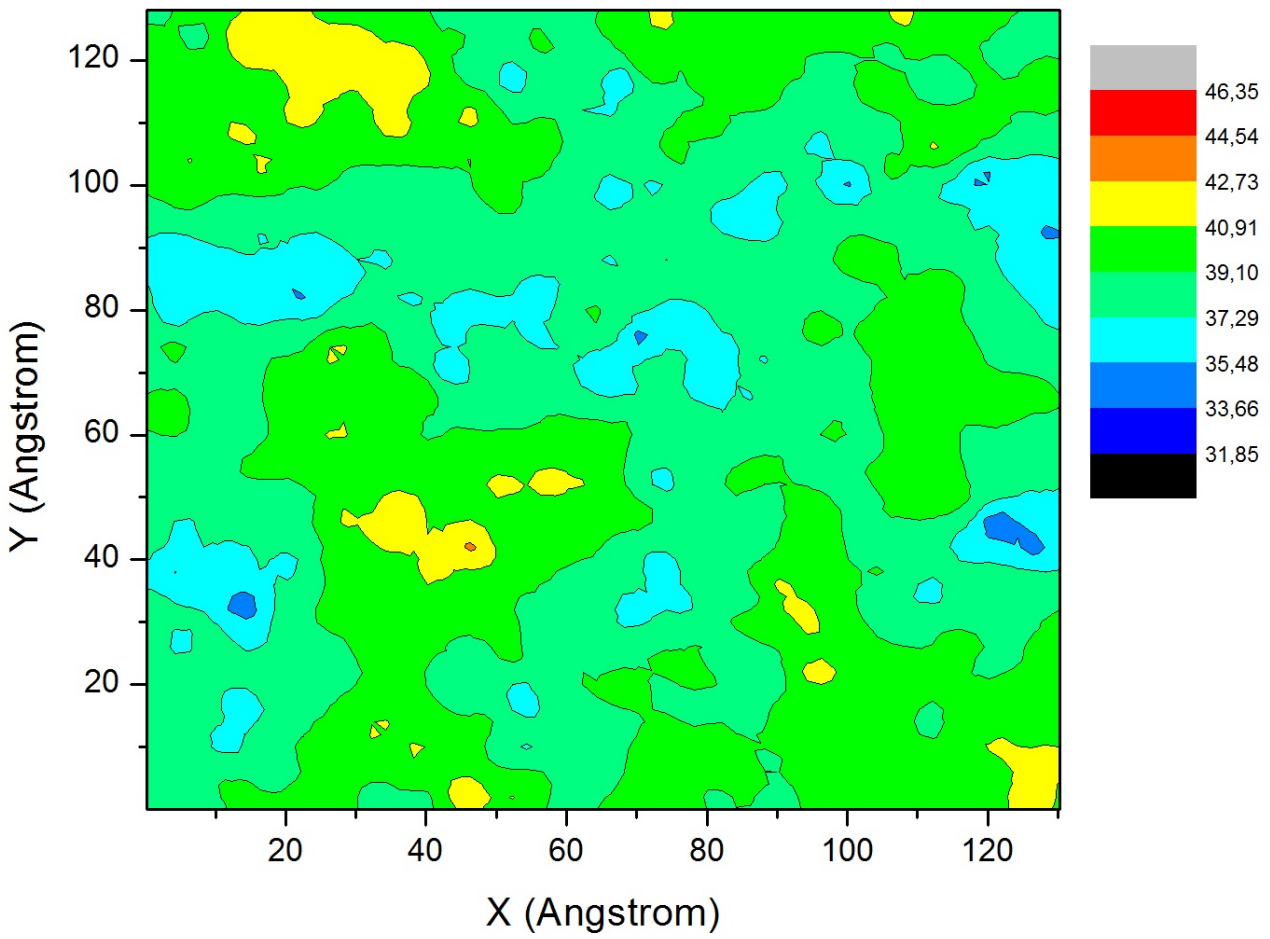

Figure S5. Thickness profile of DOPC:DOPS (7:3) lipid bilayers after 300 ns of molecular dynamic simulations.